Araştırma Makalesi / *Research Article* **Iğdır Üniversitesi Fen Bilimleri Enstitüsü Dergisi, 10(1): 214-224, 2020**
Fizik / *Physics* ***Journal of the Institute of Science and Technology,* 10(1): 214-224, 2020**

DOI: 10.21597/jist.642111 **ISSN: 2146-0574, eISSN: 2536-4618**

Electrical characterization and solar light sensitivity of SnS_2/n-Si junction

Ali BALTAKESMEZ[1*]

ABSTRACT: In this study, the SnS_2 thin film deposited by spray pyrolysis technique has been analyzed by XRD, SEM and UV-visible characterization techniques to investigate of structural, morphological and optical properties. The thin film has dominant (001) and (002) crystallographic planes, compact grain-like morphology with uniform and good coverage surface and 2.42 eV band gap. The Sn/SnS_2/Si/Au-Sb structure has been characterized by electrical measurement. The diode has ideality factor of 1.34 and barrier height of 0.762 eV with reverse-bias current temperature-dependent strongly. In addition, the ITO/SnS_2/Si/Au-Sb structure has been characterized by 1.5 AM solar simulator for determine of solar light sensitivity. The diode under 100 mW/cm^2 solar-light source has exhibited 0.24% PCE with J_{sc} of 1.83 mA/cm^2, V_{oc} of 0.46 V and FF of 0.28.

Keywords: Tin sulfide (SnS_x), Silicon, diode, sputtering, responsivity

[1] Ali BALTAKESMEZ (**Orcid ID:** 0000-0003-2175-1180), Ardahan Üniversitesi, Teknik Bilimler Meslek Yüksekokulu, Elektrik ve Enerji Bölümü, Ardahan, Türkiye

*Sorumlu Yazar/Corresponding Author: Ali BALTAKESMEZ, e-mail: alibaltakesmez@ardahan.edu.tr

Geliş tarihi / *Received:* 04-11-2019
Kabul tarihi / *Accepted:* 02-12-2019

INTRODUCTION

The binary metal-chalcogenide (M_xVI_y) semiconductor materials such as SnS, SnS_2, ZnS, CdS and In_2S_3 are important for today's technological developments due to critical and specific properties. For example, some critical properties of the materials are high optical transparency with wide band gap, controllable carrier density with metal/chalcogenide ratio, high electrical conductivity with high mobility, low ionization potential with high valence band and peculiar optical- and electrical-properties thickness-dependent with two-dimensional (2D) growth feature (Pyeon et al., 2018). Furthermore, the wide band gap chalcogenide (WBC) semiconductors are of particular importance among others for future transparent-electronic technology such as solar cell, light emitting diode and transistor applications (Johny et al., 2018).

In particular, the SnS_2 has attracted considerable interest of researchers in recent years due to n-type electrical conductivity (Kim et al., 2018), non-toxic (Dong et al., 2018), wide band gap (Huanga et al., 2017), high absorption coefficient (Chalapathi et al., 2017), high surface activity (Kumar et al., 2019), earth-abundant and cost-effective properties (Hu et al., 2019). Therefore, this material with these properties is suitable some critical opto-electronic application such as optical and transparent gas sensor for sensing NH_3, H_2S and alcohols (Anitha et al., 2018) and an buffer layer in the n-CdS/p-SnS hetero-junction solar cell instead of the CdS toxic-layer (Chalapathi et al., 2017). Furthermore, the Sn/S ratio allows change in conductivity type as p-type SnS and n-type SnS_2. Thus, the p-SnS/n-SnS_2 hetero junction solar cell or photo-sensor can be developed. A theoretical calculation revealed that the power conversion efficiency (PCE) of these solar cells can be reach 25% (Voznyi, Kosyak, Onufrijevs et al., 2016). In addition, magnetic properties at room temperature can easily be gained to 2D layered WBCs with doping magnetic atom such as Fe, Co and Ni (Li et al., 2017). These magnetic 2D layered WBC materials are suitable for applications of spintronic such as high-resolution and high-sensitivity magneto-optic microscopy. Vijayakumar et al. have studied on characterization of SnS_2 thin films prepared at different substrate temperature using spray pyrolysis technique (Vijayakumar et al., 2011). Interestingly, the film band gap has decreased from 2.80 eV to 2.6 eV with increasing substrate temperature. In addition, the electrical resistivity in dark and in light has shown significantly decrease from $5.95x10^3$ Ωcm to $2.22x10^3$ Ωcm and from $1.48x10^3$ Ωcm to $0.55x10^3$ Ωcm, respectively. This result suggests that SnS_2 thin film could be an alternative photo-active material for optical transistor channel as well as solar cell.

The SnS_2 thin films have been reported using various preparation process including thin film growth technic such as molecular beam epitaxy (MBE) (Schlaf et al., 1995), vacuum evaporation (VE) (Shi et al., 2012), spin-coating (Orletskyi et al., 2018), chemical bath deposition (CBD) (Li et al., 2011), chemical vapor-deposition (CVD) (Ye et al., 2017), plasma chemical vapor deposition (P-CVD) (Sanchez-Juarez et al., 2005) and spray pyrolysis technique (SP) (Kumar et al., 2017). Compared with other thin film deposition techniques, the SP technique allows some crucial advantages to obtain final desired material such as nano-film, clusters, porous-film and high density packaged film. In the non-vacuum SP system, controllable parameters as spray energy, gas flow pressure, sprayed drop size, substrate temperature allow the desired design and synthesis of various functional materials with composition and morphology (Leng et al., 2019).

In this study, the SnS_2 thin film has been deposited by the SP technique. The structural, morphological and optically demonstrated SnS_2 thin film has been used to obtain Sn/SnS_2/Si/Au-Sb and ITO/SnS_2/Si/Au-Sb structures. The interlayer and solar light sensitivity performance of Sn/SnS_2/Si/Au-Sb and ITO/SnS_2/Si/Au-Sb structures has been analyzed respectively.

MATERIALS AND METHODS

First, a cleaning process was applied to purify the surface of the substrate from organic impurities. While the glass substrate was cleaned with ethanol, the n-Si substrate was cleaned by using the RCA cleaning procedure (in boiling NH_3+H_2O_2+6H_2O solution for 10 min and then in HCl+ H_2O_2+6H_2O for 10 min at 60 ºC). For the Si substrate, the ohmic contact was obtained by thermally evaporating Au-Sb alloy on the back side of Si. After the deposition, the substrate was annealed at 420 ºC for 3 min in N_2 atmosphere.

Second, the SnS_2 thin film was deposited onto the Si substrate by spray pyrolysis technique. The solution was prepared using Tin (II) chloride dihydrate ($SnCl_2$:2H_2O) and thiourea ($CS(NH_2)_2$) powders from Sigma-Aldrich purchased. The thin film has been deposited using solution consist of the SnCl2·2H2O and the $CS(NH_2)_2$ in de-ionized water and 37% chloric acid, respectively. The molarities of both solutions were 0.1 M. The solution was sprayed at a 1.5 ml/min rate for 6 mins onto the pure side of Si at 350 °C. The pressure of the carrier gas (dry oxygen) is 0.7 bar and the distance between nozzle and substrate is 25 cm. The Sn metal was evaporated on SnS thin film to obtain the Sn/SnS_2/n-Si/Au-Sb structure. On the other hand, for testing solar light sensitivity, the indium tin oxide (ITO) was sputtered by RF magnetron sputtering system on the SnS_2/n-Si/Au-Sb as top transparent contact. The source material is a commercial 99.99% pure ITO target having a radius of 2 inch and thickness of 0.25 inch from Kurt J. Lesker Company. Throughout the sputtering process, 99.999% pure Ar was used as a plasma gas. The distance between target and substrate is 6 cm and RF power is 100 W. The contact area is 7.85×10^{-3} cm^2 for the both contact (Sn and ITO). The experimental process is given schematically in Figure 1.

The structural characterization was carried out by X-ray Diffraction (XRD) measurement system, Rigaku D/Max-IIIC diffractometer with Cu:Kα radiation. The surface morphology of the films was scanned by a Scanning electron microscope (SEM), Zeiss Sigma 300 instrument. Perkin-Elmer Lambda2S UV-visible spectrometer was used to obtain optical absorbance spectrum of the thin film. The I-V measurements of the device were carried out using Leybold Heraeus closed-cycle helium cryostat with KEITHLEY 487 Picoammeter/Voltage Source. In addition, the current density-voltage (J-V) characteristic under illumination were tested by a solar simulator system (Sciencetech SF300–100 mW/cm^2) under AM 1.5G one sun illumination. It is calibrated using a certified silicon reference cell, with a Keithley 2400 source-meter unit inside the glove box.

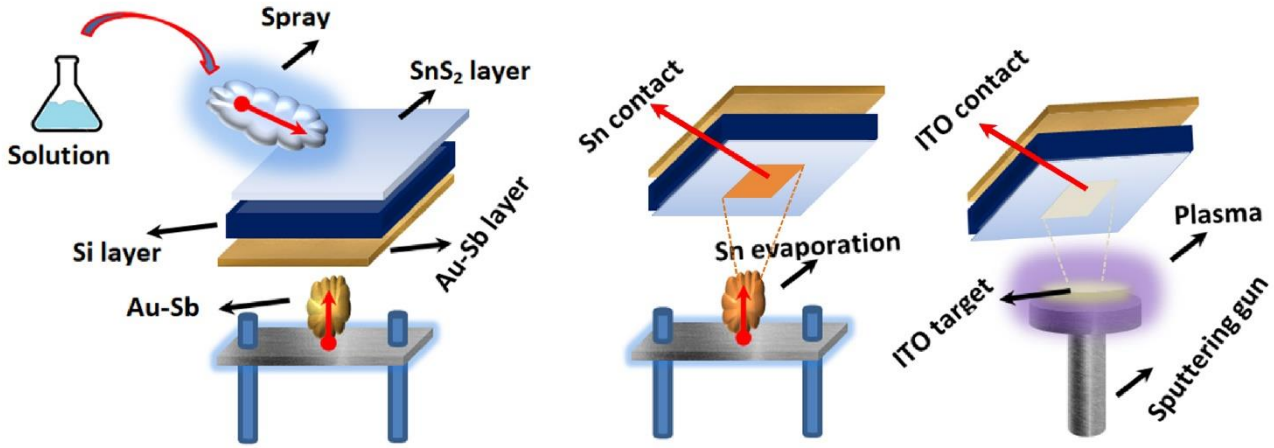

Figure 1. The schematically illustration of the experimental processes.

RESULTS AND DISCUSSION

Figure 2(a) shows XRD pattern of SnS_2 films deposited on the Si. In addition, the Figure 2(b) shows XRD pattern of the film deposited on the glass. According to the patterns, dominant peaks at 14.89º and 31.81º (at 31.69º in the film deposited on glass) correspond to reflections from the (001) and (002) crystallographic planes of hexagonal phases, respectively (Seo et al., 2017; Voznyi, Kosyak, Opanasyuk et al, 2016). The values of Full Width at Half Maximum (FWHM) of the dominant peaks have determined to obtain average grain size. The FWHM values are determined to be 2.16 and 0.17. The average crystal size is calculated from well-known Scherrer's equation,

$$D = \frac{0.9\lambda}{\beta cos\theta} \quad (1)$$

where λ the x-ray wavelength, β the value of FWHM and θ the diffraction angle of the dominant peak. The calculated average grain sizes are 3.82 nm and 50.12 nm, respectively. On the other hand, the weak peaks have been also observed at 30.64º, 38.94º, 44.51º, 47.64º,54.43º,56.13º and 66.29º correspond to reflection from (011), (311), (411), (112), (312), (321), (411) and (800) planes belong to orthorhombic structure of the SnS crystal (Reddy and Kumar, 2016, Ju et al., 2019). Besides, the (202) plane of the orthorhombic phase of Sn_2S_3 has been observed in the film deposited on glass (Voznyi et al, 2016). Furthermore, diffraction peak of (310) crystallographic plane belong to the SnO phase (Janardhan et al., 2018) has been observed at 61.66 in the films deposited on the Si. The SnO may be form in interface between Si and SnS_2 due to oxides surface of Si and/or high amount of Sn in the solution. The Sn element has high reaction potential with oxygen and thus the excess elements are reacted with oxygen to form the SnO phase (Chen et al., 2008).

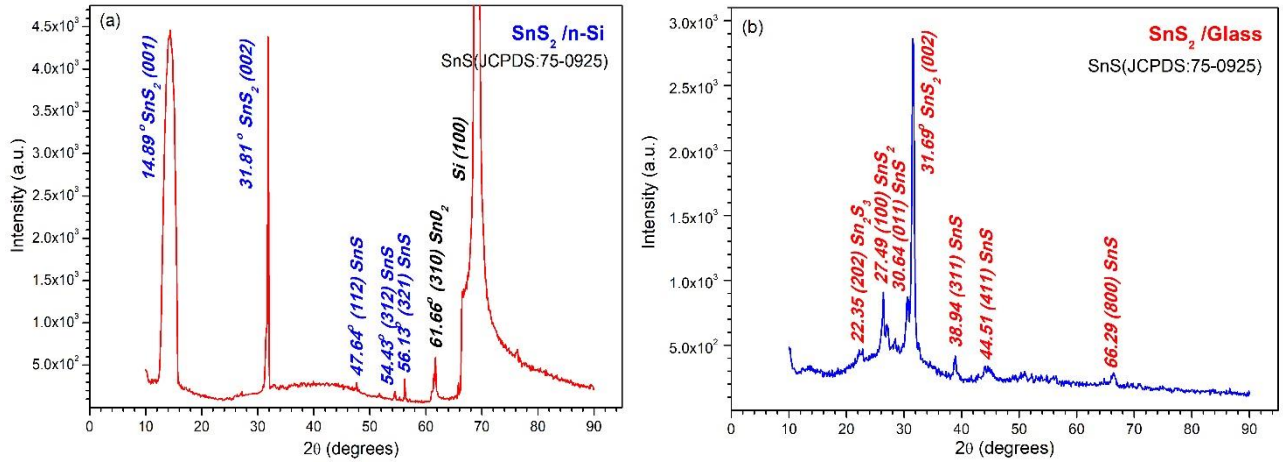

Figure 2. XRD patterns of the SnS_2 thin film deposited on the Si (a) and glass (b) substrates.

The morphology of the top surface of the SnS_2 thin film is presented with SEM image in Figure 3. The image shows a compact grain-like growth with uniform and good coverage surface morphology. In the solution based process, substrate, solution and annealing temperatures are crucial parameters for crystallinity and morghology. For example, the surface morghology features of as-deposited and annealed SnS_x thin films have been reported (Reddy et al., 2018) and the cross-sectional view and SEM image showed that the annealing temperature has caused changing morphology with increasing temperature from 300 ºC to 400 ºC. The morphology has a hexagonal flake-like structure at 300 ºC , a

completely covered hexagonal flakes at 350 ºC and cylindrical nanorod-like structures at 400 ºC. Furthermore, increasing temperature has also caused phase transition from SnS_2 to SnS after 500 ºC. In another report, the SnS_2 thin films have been prepared in two different solvent (ethanol and isopropyl alcohol) and investigated effet of annealing temperature (Johny et al., 2018). While the effect of solvent has been observed to be morphological defects such as porosity and pinholes, the effect of temperature is caused different surface morphology such as compact nanocolloid and nanoparticle. Clearly, the SEM image and the XRD patterns are quite compatible with each other due to the hexagonal crystal structure of SnS_2 with average grain size of 50.12 nm observed in the XRD patterns.

Figure 4 shows the plot of $(\alpha h\upsilon)^2$ versus photon energy ($h\upsilon$) obtained by optic-absorption spectrum of the SnS_2 thin film in range of 300 nm and 900 nm, as seen in inset figure. The film has an optical absorption onset at 550 nm with sharp absorption edge. The band gap (E_g) value has been determined to be 2.42 eV for direct allowed transition. Futhermore, the thin film has exhibited an absorption coefficient (α) of 10^4 cm^{-1}. The E_g value has been reported around 1.3 eV for SnS and 2.4 for SnS_2 thin film (Seo et al., 2017; Wang et al., 2017). Therefore, the E_g and α values of the SnS_2 thin film are in good aggreement with those reported previously (Reddy et al., 2018). On the other hand, in order to be used as window layer or transparent charge-carrier transport layer in solar cells, the SnS_2 thin film has an advantage that the band gap can be adjusted to application-specific values. For example, Neodymium (Nd) doped SnS_2 thin films have been reported that the band gap has increased from 2.75 eV to 2.95 eV with increasing doping concentration (Arulanantham et al., 2019).

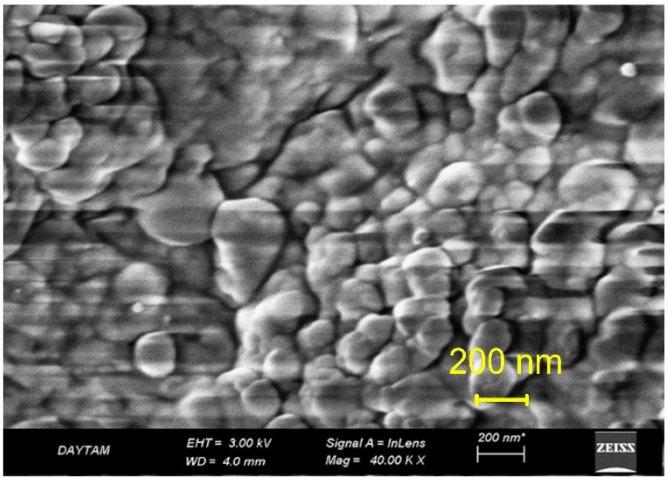

Figure 3. The surface SEM nanograph of the SnS_2 thin film.

Figure 5(a) shows the In(I)-V curves of the Sn/SnS_2/n-Si/Au-Sb diode at different temperatures. As seen in forward-bias current curve, the saturation current has increased from 10^{-6} A to 10^{-3} A with increasing temperature. However, the rectification ratio at ±1 V has not changed due to increasing reverse leakage current with increasing temperature. The directly proportional increase between reverse- and forward-bias current with increasing temperature is due to the suppressed trap-assisted tunneling current and dominant thermionic field emission current at low temperatures (Fang et al., 2009). This may be resulted that the SnO formed in interface between Si and SnS_2 as above mentioned.

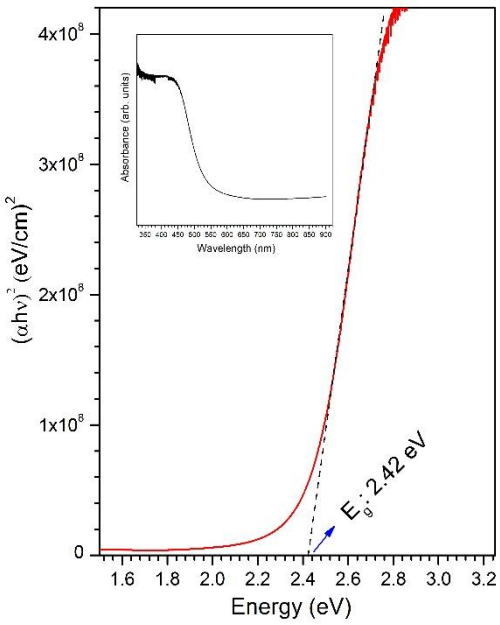

Figure 4. The plot of $(\alpha h\upsilon)^2$ versus photon energy ($h\upsilon$) of the thin film. Inset shows UV-visible absorption spectrum.

As shown in Figure 5(b) and (c), logarithmic current-voltage curves have changed with changing current-voltage mechanism at different temperatures. The three regions having different slope value are called as the ohmic current-voltage mechanism (Region I), space charge limited current (SCLC) mechanism (Region II) and trap-free SCLC mechanism (Region III) (Baltakesmez, 2019), as seen in Figure 5(c). In the region I, the ohmic current-voltage mechanism based on carrier mobility with proportional to the electric field has not been observed at low temperature and the mechanism has an onset from the SCLC ($I\text{-}V^2$). The trap-free limit voltage (V_{TFL}) is given as Eq. (2) (Kumar et al., 2008).

$$V_{TFL} = 0.5\frac{qH_b^{'}d^2}{\varepsilon\varepsilon_0} \tag{2}$$

where q is the elementary charge, d is the sample thickness, ε is the dielectric constants of the material, ε_o is the permittivity of the free-space and H_b' is the total filled trap density. According to the Eq. (2), the V_{TFL} value is directly related with total trap density. As can be seen in Figure 5(b) and (c), the voltage values have shifted from 0.49 V at 100 K to 0.38 V at 300 K. This alteration in the V_{TFL} values can be attributed that the fixed charge density in the traps depends on the temperature. Furthermore, these charges may be produce a reverse voltage in the material and thus voltage drop can be observed (Kumar et al., 2008). Therefore, in the low temperature, the presence of the SnO insulator-interface and insufficient thermal energy has caused almost zero current (~10^{-9} A) with poor mobility up to 0.2 V.

The changes in turn-on voltage and leakage current with measurement temperature have been shown in Figure 6(a). The reverse leakage current temperature-dependent behaviour is attributed to change in electron tunneling rate from traps with temperature (Pipinys et al, 2006). On the other hand, the turn-on voltage has three different change ranges and first two ranges have increased with increasing temperature up to 240 K. However, at temperatures above 220 K, the voltage is almost constant. The presence of these three different ranges of variation is due to the strongly dependent temperature dependence of the reverse-bias character of the diode. Clearly, this is a result of the temperature

dependence of the leakage current. Figure 6(b) shows plot of change in ideality factor and zero-bias barrier height (SBH), which has been calculated by the TE theory, versus temperature.

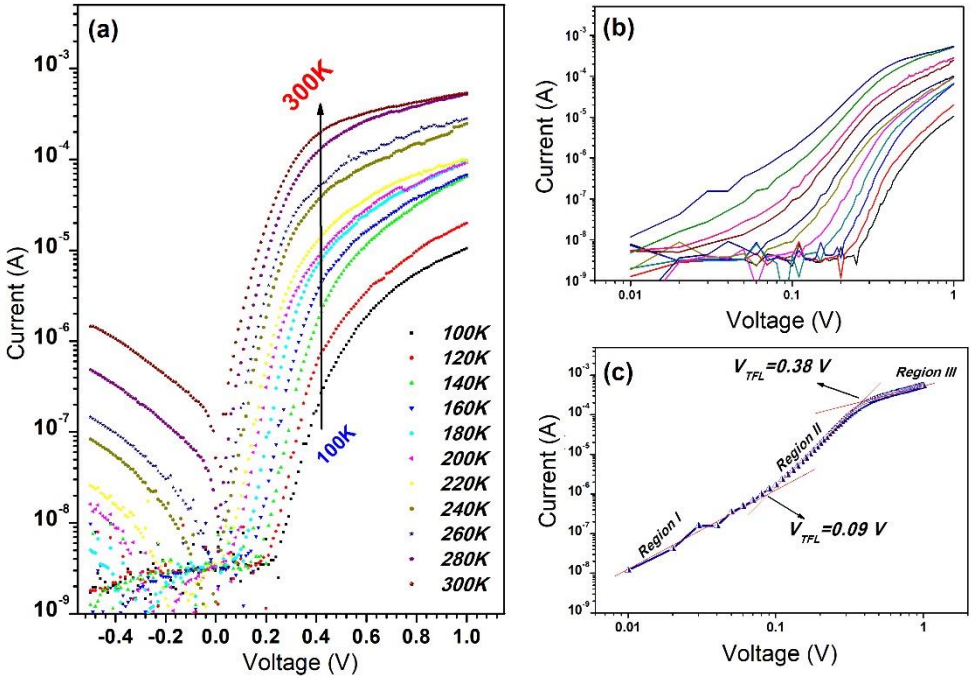

Figure 5. I-V characteristics of the diode at various temperatures; (a) log(I)-lin(V), (b) log(I)-log(V). (c) Plot of log(I)-log(V) at 300 K.

The I-V characteristics of the diode have been examined according to TE (Rhoderick and Williams, 1988). According to this theory, the current-voltage relationship is as given in Eq. (2).

$$I = I_0 \exp\left(\frac{eV}{nkT}\right)\left[1-\exp\left(-\frac{e(V-IR_s)}{kT}\right)\right] \tag{3}$$

where n is the ideality factor, k is the Boltzmann constant, e is the electron charge, V is the forward bias voltage, T is the temperature, R_s the series resistance and I_0 is the saturation current. Besides, the saturation current is as given in Eq. (3).

$$I_0 = AA^*T^2 \exp\left(-\frac{e\Phi_b}{kT}\right) \tag{4}$$

A^*, A, Φ_b are the effective Richardson constant of 112 A/cm^2K^2 for n type Si, the area of the rectifier contact, the experimental zero bias barrier height, respectively. The value of ideality factor n is can be determined from Eq. (2) as,

$$n = \frac{e}{kT}\frac{dV}{d(\ln I)} \tag{5}$$

According to the TE theory, the ideality factor has decreased with increasing temperature, changing range from 3.69 to 1.34. The calculated values have been given in Table 1. The temperature dependence of ideality factor has been frequently explained by presence of SBH inhomogeneity (Hudait and Krupanihi, 2001). In the diode, the presence of the SnS_2 interlayer and SnO interface may causes multi-surface polarity and also increases surface roughness with consist of crystal domain boundaries. Thus, these effects may cause the inhomogeneity of the SBH (Zhou et al., 2019). On the other hand, Zhou et al. have shown that the peak of bent conduction band increases with increasing forward-bias and shifts away from interface region towards the semiconductor (Zhou et al., 2019). Furthermore, these changes cause an increase in effective SBH with more uniform interface. Therefore, the change in barrier height has shown decreasing alteration with increasing temperature.

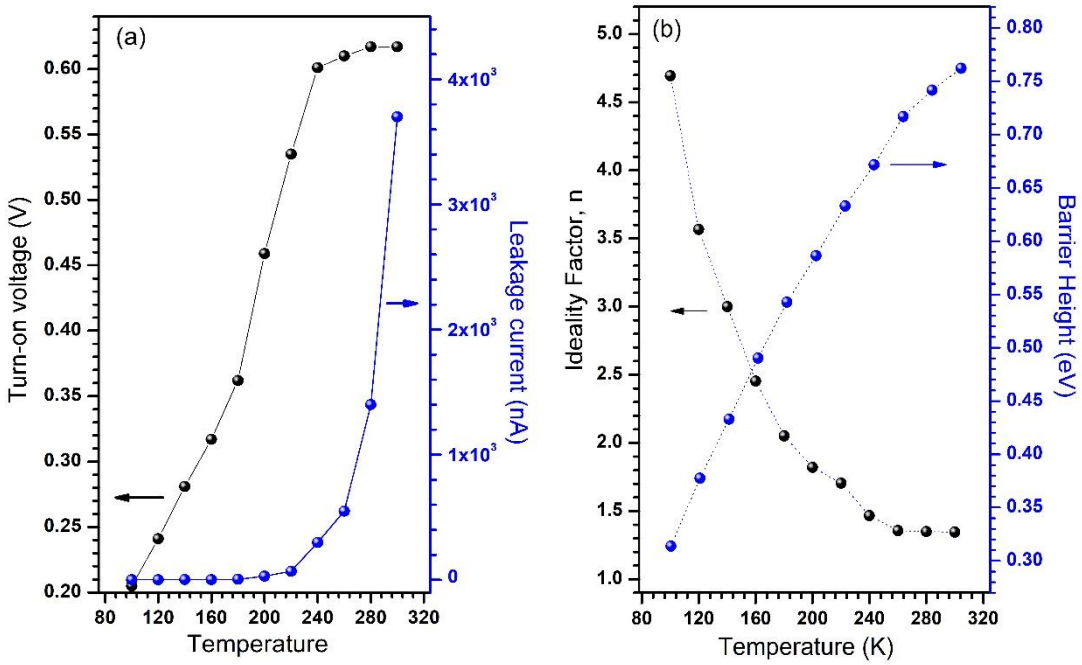

Figure 6. The plots of (a) the turn-on voltage and leakage current versus temperature and (b) the plots of ideality factor and barrier height versus temperature.

Table 1. The basic parameters of the diode.

Temp.	TE theory	
	n	Φ_b
100	3.69	0.313
120	3.56	0.377
140	3.00	0.433
160	2.45	0.490
180	2.05	0.542
200	1.82	0.586
220	1.70	0.633
240	1.46	0.671
260	1.35	0.717
280	1.34	0.741
300	1.34	0.762

Recently, Wang et al. have reported effect of the SnS_2 secondary phase on surface of Cu_2ZnSnS_4 (CZTS) thin film in solar cell having SnS_2/CZTS structure and also CdS/CZTS structure for comparatively investigation (Wang et al., 2017). In this study reported, the SnS_2 layer is not suitable for this solar cell configuration and thus, Wang et al. have introduced mechanical exfoliation (ME) as a promising method for eliminate the detrimental effect of sheet-like SnS_2 films. However, Joshi et al. have presented synthesis of SnS_2 thin film by simple arrested precipitation technique for solar cell application and the photo-electrochemical solar cell performance of SnS_2 thin films has been given to be 0.053% (Joshi et al., 2018). In another study, Chu et al. have reported locally gated SnS_2/hBN thin film transistors with a broadband photo-response (Chu et al., 2018) and demonstrated a high photo-responsivity of ~0.7 mA/W in the SnS_2 channel transistor. Clearly, the SnS_2 thin film has an important application potential in suitable device fabrication. Therefore, to investigation of the performance of solar light sensitivity, the ITO/SnS_2/n-Si/Au-Sb structure has been measured under 1.5 AM light spectrum. The I-V characteristic of the diode has shown a solar cell character as seen in Figure 8. The device has exhibited a short-circuit current density (J_{sc}) of 1.83 mA/cm^2, an open-circuit voltage (V_{oc}) of 0.46 V and a fill factor (FF) of 0.28 and then PCE of 0.24%. Although low efficiency has been obtained due to high series resistance and low shunt resistance, as seen in I-V character, this promising performance may be improved with investigation detailed SnS_2 and contact properties.

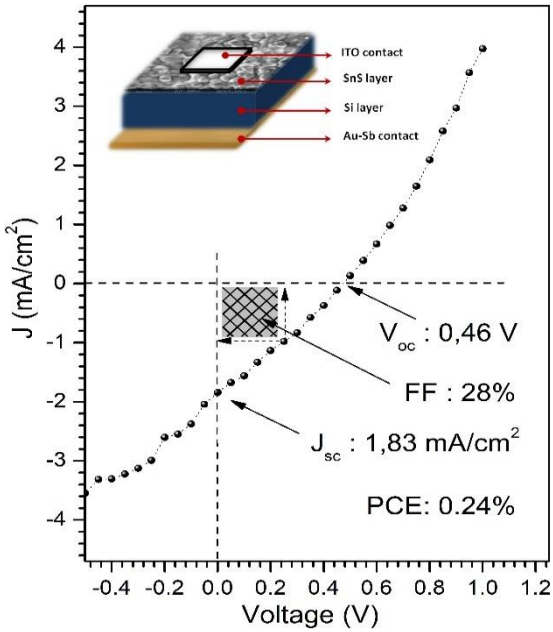

Figure 8. The current density-voltage characteristic of the diode under 1.5 AM solar light.

CONCLUSION

Consequently, the SnS_2 thin film having large grain size (>200 nm in the SEM image) and wide band gap (~2.4 eV) has been deposited by spray pyrolysis technique on the Si and glass substrates. The predominant growth plane and average grain size has been determined to be (002) and ~50 nm from the XRD pattern. The Sn/SnS_2/Si/Au-Sb diode structure prepared by thermally evaporated metal contact has been achieved with ideality factor of 1.34 and barrier height of 0.762 eV. The ITO/SnS_2/Si/Au-Sb structure prepared by RF sputtered ITO contact has solar light sensitivity. The diode under 100 mW/cm^2 solar-light source has been exhibited 0.24% PCE with J_{sc} of 1.83 mA/cm^2, V_{oc} of 0.46 V and FF of 0.28.

ACKNOWLEDGEMENT

I acknowledge the assistance of Dr. B. Güzeldir (Atatürk University) in preparation of the thin film.

REFERENCES

Anitha N, Anitha M, Mohamed J R, Valanarasu S and Amalraj L, 2018, Influence of tin precursor concentration on physical properties of nebulized spray deposited tin disulfide thin films, Journal of Asian Ceramic Societies 6, 2, 121–131.

Arulanantham A M S, Valanarasu S, Rex Rosario S, Kathalingam A, Shkir Mohd., Ganesh V., I. S. Yahia I G, 2019, Investigation on nebulizer spray coated Nd-doped SnS2 thin films for solar cell window layer application, Journal of Materials Science: Materials in Electronics 30: 13964.

Baltakesmez A, 2019, Improved barrier parameters and working stability of Au/p-GO/n-lnP/Au–Ge Schottky barrier diode with GO interlayer showing resistive switching effect, Vacuum 168 108825.

Chalapathi U, Poornaprakash B, Purushotham Reddy B P and Park S-H, 2017, Preparation of SnS2 thin films by conversion of chemically deposited cubic SnS films into SnS2, Thin Solid Films 640, 81–87.

Chalapathi U, Poornaprakash B, Reddy B P, Park S-H, 2017, Preparation of SnS2 thin films by conversion of chemically deposited cubic SnS films into SnS2, Thin Solid Films 640, 81–87.

Chen W, Ghosh D and Chen S, 2008, Large-scale electrohemical synthesis of SnO2 nanoparticles, Journal of Materials Science, 43:5291-5299

Chu D, Pak S W and Kim E K, 2018, Locally Gated SnS2/hBN Thin Film Transistors with a Broadband Photoresponse, Scientific Reports, 8:10585.

Dong Y, Cai G, Zhang Q, Wang H,Zhe Sun Z, Wang H, Wang Y and Xue S, 2018, Solution-phase deposition of SnS thin films via thermo-reduction of SnS2, Chem. Commun.,54, 1992-1995.

Fang L, Tao W, Bo S, Sen H, Fang L, Nan M, Fu-Jun X, Peng W and Jian-Quan Y, 2009, The leakage current mechanisms in the Schottky diode with a thin Al layer insertion between Al0.245Ga0.755N/GaN heterostructure and Ni/Au Schottky contact, Chinese Physics B, 18(04), 1614-04.

Hu W, Hien T T, Kim D and Chang H S, 2019, Enhancement in Photoelectrochemical Performance of Optimized Amorphous SnS2 Thin Film Fabricated through Atomic Layer Deposition, Nanomaterials 2019, 9, 1083.

Huanga P-C, Wang H-I, Brahma S, Wang S-C and Huang J-L, 2017, Synthesis and characteristics of layered SnS2 nanostructures via hot injection method, Journal of Crystal Growth 468, 162–168.

Hudait M K and Krupanidhi S B, 2001, Doping dependence of the barrier height and ideality factor of Au/n-GaAs Schottky diodes at low temperatures, Physica B Condensed Matter 307(1-4):125-137.

Janardhan E, Reddy M M, Reddy P V and Reddy M J, 2018, Synthesis of SnO Nanoparticles-A Hydrothermal Approach, World Journal of Nano Science and Engineering, 8:33-37.

Johny J, Guzman S S, Krishnan B, Avellaneda D A, Shaji S, 2018, Nanostructured SnS2 Thin Films from Laser Ablated Nanocolloids: Structure, Morphology, Optoelectronic and Electrochemical Properties, ChemPhysChem, 19, 2902 – 2914.

Joshia M P, Khota K V, Ghanwata V B, Kharadea S D, Bagadea C S, Desaia N D, Patila S S and Bhosale P N, 2018, Synthesis of tin sulphide thin film by simple arrested precipitation technique for solar cell application, AIP Conference Proceedings 1989, 020015.

Ju H, Park D, Kim J, 2019, Conductive polymer based high-performance hybrid thermoelectrics: Polyaniline/tin(II) sulfide nanosheet composites, Polymer 160 24–29.

Kim J, Kim J, Yoon S, Kang J-Y, Jeon C-W and Jo W, 2018, Single Phase Formation of SnS Competing with SnS2 and Sn2S3 for Photovoltaic Applications: Optoelectronic Characteristics of Thin-Film Surfaces and Interfaces, The Journal of Physical Chemistry C, 122, 6, 3523-3532.

Kumar G M, Ilanchezhiyan P, Cho H D, Yuldashev S, Jeon H C, Kim D Y and Kang T W, 2019, E_ective Modulation of Optical and Photoelectrical Properties of SnS2 Hexagonal Nanoflakes via Zn Incorporation, Nanomaterials 2019, 9, 924.

Kumar K D A, Valanarasu S, Tamilnayagam V and Amalraj L, 2017, Structural, morphological and optical properties of SnS2 thin films by nebulized spray pyrolysis technique, J Mater Sci: Mater Electron 28: 14209.

Kumar P, Jain S C, Kumar V, Chand S and Tandon R P, 2008, Trap filled limit and high current–voltage characteristics of organic diodes withnon-zero Schottky barrier, Journal Of Physics D: Applied Physics 41155108.

Leng J, Wang Z, Wang J, Wu H-H, Yan G, Li X, Guo H, Yong Liu Y, Zhang Q and Guo Z, 2019, Advances in nanostructures fabricated via spray pyrolysis and their applications in energy storage and conversion, Chem. Soc. Rev., 48, 3015-3072.

Li B, Xing T, Zhong M, Huang L, Lei N, Zhang J, Li J and Wei Z, 2017, A two-dimensional Fe-doped SnS2 magnetic semiconductor, Nature Communications, 8: 1958.

Li J, Zhang Y C and Zhang M, 2011, Preparation of SnS2 Thin Films by Chemical Bath Deposition, Materials Science Forum, 663-665, pp. 104-107.

Orletskyi I G, Solovan M M, Maryanchuk P D, Maistruk E V, Pinna F, Tresso E and Brus VV, 2018, Optical properties of spin-coated SnS2 thin films, Proc. SPIE 10612, Thirteenth International Conference on Correlation Optics, 106120P (18 January 2018).

Pipinys P and Lapeika V, 2006, Temperature dependence of reverse-bias leakage current in GaN Schottky diodes as a consequence of phonon-assisted tunneling, Journal of Applied Physics 99, 093709.

Pyeon J J, Baek I-H, Lim W C, Chae K H, Han S H, Lee G Y, Baek S-H, Kim J-S, Choi J-W, Chung T-M, Han J-H, Kang C-Y and Kim S K, 2108, Low-temperature wafer-scale synthesis of two-dimensional SnS2, Nanoscale,10, 17712-17721.

Reddy P P, Chandra Sekhar M, Prabhakar Vattikuti S V, Suh Y, Park S-H, 2018, Solution-based spin-coated tin sulfide thin films for photovoltaic and supercapacitor applications, Materials Research Bulletin 103 13–18.

Reddy T S and Kumar M S, 2016, Co-evaporated SnS thin films for visible light protodedector applications, RSC Advances, 6:95680-95692.

Rhoderick E H and Williams R H, 1988, Metal-Semiconductor Contacts, (Oxford: University Press, 1988)

Sanchez-Juarez A, Tiburcio-Silver A and Ortiz A, 2005, Fabrication of SnS2/SnS hetero-junction thin film diodes by plasma-enhanced chemical vapor deposition, Thin Solid Films 480–481,452–456.

Schlaf R, Louder D, Lang O, Pettenkofer C, Jaegermann W, Nebesny K W, Lee A, Parkinson B A and Armstrong N R, 1995, Molecular beam epitaxy growth of thin films of SnS2 and SnSe2 on cleaved mica and the basal planes of single-crystal layered semiconductors: Reflection high-energy electron diffraction, low-energy electron diffraction, photoemission, and scanning tunneling microscopy/atomic force microscopy characterization, Journal of Vacuum Science & Technology A 13, 1761.

Seo W, Shin S, Ham G, Lee J, Lee S, Choi H and Jeon H, 2017, Thickness-dependent structure and properties of SnS2 thin films prepared by atomic layer deposition, Japanese Journal of Applied Physics 56, 3, 031201.

Shi C, Chen Z, Shi G, Sun R, Zhan X and Shen X, 2012, Influence of annealing on characteristics of tin disulfide thin films by vacuum thermal evaporation, Thin Solid Films 520, 4898–4901.

Vijayakumar K, Sanjeeviraja C, Jayachandran M and Amalraj L, 2011, Characterization of Tin disulphide thin films prepared at different substrate temperature using spray pyrolysis technique, J Mater Sci: Mater Electron 22: 929–935.

Voznyi A, Kosyak V, Onufrijevs P, Grase L, Vecstaudza J, Opanasyuk A, Medvid A, 2016, Laser-induced SnS2-SnS phase transition and surface modification in SnS2 thin films, Journal of Alloys and Compounds 688, 130-139.

Voznyi A, Kosyak V, Opanasyuk A, Tirkusova N, Grase L, Medvids A, Mezinskis G, 2016. Structural and electrical properties of SnS2 thin films. Materials Chemistry and Physics 173, 52-61.

Wang W, Chen G, Cai H, Chen B, Yao L,Yang M, Chen S and Huang Z, 2017, The effects of SnS2 secondary phases on Cu2ZnSnS4 solar cells: a promising mechanical exfoliation method for its removal, Journal of Materials Chemistry A,6, 2995-3004.

Ye G, Gong Y, Lei S, He Y, Li B, Zhang X, Jin Z, Dong L, Lou J, Vajtai R, Zhou W and Ajayan P M, 2017, Synthesis of large-scale atomic-layer SnS2 through chemical vapor deposition, Nano Research, 10(7): 2386–2394.

Zhou Q, Wu H, Li H, Tang X, Qin Z, Dong D, Lin Y, Lu C, Qiu R, Zheng R, Wang J and Li B, 2019, Barrier Inhomogeneity of Schottky Diode on Nonpolar AlN Grown by Physical Vapor Transport, IEEE Journal of the Electron Devices Society (7), 662 – 667.